Phase transitions in a multiple quantum well in strong magnetic fields

Xiu Qiu and Robert Joynt
Department of Physics, University of Wisconsin–Madison, 1150 University Avenue, Madison, Wisconsin 53706
and Institute for Theoretical Physics, University of California, Santa Barbara, California 93106

A. H. MacDonald
Department of Physics, Indiana University, Bloomington, Indiana 47405
(Received 30 October 1989)

We study the phases of a multiple-quantum-well system of layered two-dimensional electrons in a strong perpendicular magnetic field. Solid phases are found at small fillings of the lowest Landau level which are the hexagonal-close-packed lattice at large interlayer separations and the body-centered-tetragonal lattice at small separations. We find that a sequence of incompressible-Laughlin-liquid-like states occurs at larger fillings. The energies and correlation functions of these states have been calculated by using Monte Carlo simulations. We also discuss the quasiparticle and collective excitations of the liquid states. We find that the electric charge carried by a quasiparticle can have a contribution in one layer which is an irrational fraction of the electron charge. It should be possible to observe the transitions between different Laughlin-like phases experimentally. Transport and microwave experiments are particularly promising in this regard.

I. INTRODUCTION

There has been intensive investigation of the fractional quantum-Hall effect[1] since it was discovered a few years ago. It is believed on theoretical grounds that the incompressible-Laughlin-liquid state[2] will solidify to a Wigner crystal when the density of the two-dimensional electrons becomes small.[3] This occurs for electrons on the surface of liquid helium.[4] There is evidence for this in a semiconductor system in a recent experiment.[5] In a recent brief paper,[6] we catalogued the different solid phases that occur in a layered system. In addition, and more importantly, we found a sequence of liquid phases which exhibit the fractional quantum-Hall effect. These phases are extensions of the Laughlin state to three dimensions. The observation of the integral quantum-Hall effect in three-dimensional systems[7] makes this extension of experimental relevance.

The system we consider is a multiple quantum well consisting of layers each containing a two-dimensional electron gas (2D EG). The whole system is placed in a strong magnetic field perpendicular to the layers. The layers are taken to be infinitely thin and neighboring layers are separated by a distance d. They interact with each other through the long-range Coulomb potential without conduction between the layers, unlike the system of Ref. 7 where tunneling between layers takes place. We assume that the magnetic field is strong enough that the electrons reside in the lowest Landau level and in one spin state only. Possible quantum-Hall states in a two-layer system have been studied by exact diagonalization of a small system of eight electrons.[8] In this paper we concentrate on a system with an infinite number of layers and the new features that arise in this case.

Our calculations show that even when there is no conduction between the layers, a rich variety of phases appear. The zero-temperature phase diagram we constructed is shown in Fig. 1. When the Landau filling factor ν is small, the ground states are Wigner crystals. The hexagonal-close-packed (hcp) structure at large interlayer separation d is followed by a body-centered-tetragonal (bct) structure at small d. At larger fillings, we get a series of Laughlin-liquid-like states. These liquid states have quasiparticle excitations which localize an irrational

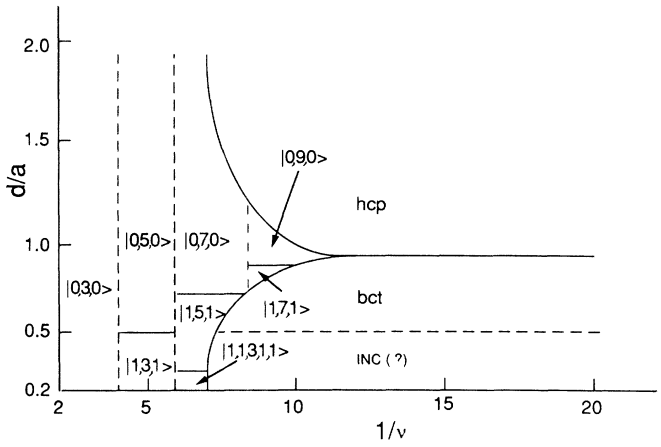

FIG. 1. Phase diagram of the multiple quantum well as a function of layer spacing and two-dimensional electron density. hcp and bct denote hexagonal-close-packed and body-centered-tetragonal Wigner lattices. INC denotes an incommensurate density wave. $|b,a,b\rangle$ are liquid states whose definitions are given in the text. States whose precise structure we have not been able to determine are marked with a query. Dashed phase boundaries are those whose exact positions are not known.

amount of charge in a layer. At very small separations, a staging transition occurs.[9]

To observe the fractional quantum-Hall effect, high-quality semiconductor systems with mobility $\sim 10^6$ cm^2/V sec are required. Recent advances in the fabrication of $GaAs/Al_xGa_{1-x}As$ structures make it seem likely that the observation of the fractional quantum-Hall effect in a multiple-quantum-well system will soon be experimentally feasible.

In this paper, we show in detail how we determined the ground-state energy of both the liquid and solid states in order to construct the phase diagram. We also discuss the properties of the ground state and both the quasiparticle and collective excitations of the liquidlike states.

In Sec. II we determine the ground-state energy of the liquid states by using Monte Carlo techniques. The energies of the solid states, including higher-stage states, are discussed in Sec. III. We discuss in Sec. IV the pair correlation functions of the liquid states, which were also obtained by Monte Carlo simulations. Then we turn to the excitation properties of the liquid states. We examine the quasiparticle excitations in Sec. V and the collective excitations in Secs. VI–IX. Section X concludes the paper with suggestions for the experimental determination of the phase diagram.

II. GROUND-STATE ENERGY OF THE LIQUID STATES

Let us first look at the liquid phases. When the interlayer separation d is large compared with $a=\rho^{-1/2}$ (where ρ is the electron density in the layer), correlations between different layers are weak. We may express the wave function of our layered system as a direct product of the two-dimensional Laughlin wave functions for each layer at $\nu=1/m$ filling:

$$|0,m,0\rangle=\exp\left[-\sum_{i=1}^{N}\sum_{\alpha=1}^{M}|z_{i\alpha}|^2/4l^2\right]\prod_{\alpha=1}^{M}\prod_{1\le i<j\le N}(z_{i\alpha}-z_{j\alpha})^m , \tag{2.1}$$

where $z_{i\alpha}=x_{i\alpha}-iy_{i\alpha}$, $(x_{i\alpha},y_{i\alpha})$ is the position of the ith electron in the αth layer. $i=1,2,\ldots,N$. $\alpha=1,2,\ldots,M$. Here N is the number of electrons in each layer, M the number of layers, and $l=(\hbar c/eB)^{1/2}$ is the magnetic length. There is a hierarchy of incompressible-liquid states at filling factors p/m, where p and m are integers and m is odd. Here we only consider the states corresponding to $p=1$ since the exact form of the states with large p is not known even in two-dimensional cases. We also omit discussing the even-denominator states. They are unlikely to appear when electrons only occupy the lowest Landau level. (The even-denominator effects observed so far[10] correspond to filling factor $\nu>2$.)

At small separation d, correlations between different layers must be taken into account. We proposed a correlated wave function including the correlations between neighboring layers. It is a generalization of Halperin's two-component wave function[11] to the case of many two-dimensional (2D) layers.

Our first type of correlated wave function can be expressed as

$$|1,s,1\rangle=\exp\left[-\sum_{i=1}^{N}\sum_{\alpha=1}^{M}|z_{i\alpha}|^2/4l^2\right]\prod_{\alpha=1}^{M}\left[\prod_{1\le i,j\le N}(z_{i,\alpha-1}-z_{j\alpha})\prod_{1\le i<j\le N}(z_{i\alpha}-z_{j\alpha})^s\right] , \tag{2.2}$$

where s is an odd integer.

This state has the characteristic of keeping the electrons in neighboring layers apart while at the same time retaining the intralayer correlations. The square of the wave function can be interpreted as the classical partition function of a many-component plasma with different interactions among the various components. It is an incompressible liquid for $s>1$. For $s=1$, it is unstable, as we shall show below. The electrons are uniformly distributed within each layer. The electron density is given by $\rho=\nu/2\pi l^2$. The corresponding filling factor is $\nu=1/(s+2)$, the same as in the $|0,s+2,0\rangle$ state. The $|1,s,1\rangle$ ground state will be preferred once the interlayer interactions become sufficiently strong.

The second type of correlated wave function that we study is defined by

$$|1,1,s,1,1\rangle=\exp\left[-\sum_{i=1}^{N}\sum_{\alpha=1}^{M}|z_{i\alpha}|^2/4l^2\right]\prod_{\alpha}\left[\prod_{1\le i,j\le N}(z_{i,\alpha-1}-z_{j\alpha})(z_{i,\alpha-2}-z_{j\alpha})\prod_{1\le i<j\le N}(z_{i\alpha}-z_{j\alpha})^s\right] . \tag{2.3}$$

This wave function explicitly includes correlations between second-neighbor layers as well as nearest neighbors. It will have lower energy than the first kind of correlated state when the interlayer separation decreases further, that is, when the interlayer correlation plays a more important role.

The wave functions we have introduced can also be discussed using the nonvariational pseudopotential approach of Haldane.[12] The interaction potential between particles (i,α) and $(j,0)$ may be written as

$$V(\mathbf{r}_{i\alpha}-\mathbf{r}_{j0})=\frac{1}{\pi}\int d^2Q\sum_{m=0}^{\infty}V_m^{\alpha}L_m(Q^2)\exp[i\mathbf{Q}\cdot(\mathbf{r}_{i\alpha}-\mathbf{r}_{j0})]\exp(-Q^2/2) ,$$

where

$$V_m^{\alpha}=\int_0^{\infty}dQ\,QL_m(Q^2)\exp(-Q^2)\frac{1}{2\pi}\int d^2r\exp(i\mathbf{Q}\cdot\mathbf{r})V^{\alpha}(\mathbf{r}) .$$

Here $V^{\alpha}(\mathbf{r})$ is the interaction, assumed repulsive, of particles in layers separated by αd, and $m \geq 0$ labels the z component of the relative angular momentum of two particles. L_m is the mth Laguerre polynomial. Following Haldane, we note that in the wave function $|0,m_0,0\rangle$, electrons in the same layer never have angular momentum $m < m_0$. This wave function would therefore be an exact solution for an interaction for which $V_m^0 = 0$, $m \geq m_0$ and $V_m^{\alpha} = 0$, $|\alpha| \geq 1$. Similarly, the wave function $|1,s,1\rangle$ would be the exact solution if $V_m^0 = 0$, $m \geq s$, $V_m^1 = 0$ for $m \geq 1$, and $V_m^{\alpha} = 0$ for $|\alpha| \geq 2$. As d is reduced, V_0^1 increases and eventually becomes larger than V_m^0 for some value of m. In this case one might expect $|1,m_0,1\rangle$ to become stable with respect to $|0, m_0+2, 0\rangle$ since the energy gained by avoiding relative angular-momentum zero between electrons in neighboring layers exceeds the energy cost of introducing relative angular-momentum m_0 within a layer. This allows us to make a quantitative prediction of the phase boundary, since we can compare the relative magnitude of V_0^1 and $V_{m_0}^0$. For the Coulomb interaction,

$$V_m^{\alpha} = \int_0^{\infty} dQ\, QL_m(Q^2)\exp(-Q^2)\left[\frac{1}{2\pi}\right] \times \int d^2r \exp(i\mathbf{Q}\cdot\mathbf{r})(r^2+\alpha^2d^2)^{-1/2} .$$

The case of most interest is $m_0 = 3$, for which the value $V_3^0 = 5\sqrt{\pi}/32 = 0.28$.

$$V_0^1 = (\sqrt{\pi}/2)\exp(d^2/4l^2)\mathrm{erfc}(d/2l) ,$$

where erfc(x) is the complementary error function:

$$\mathrm{erfc}(x) = \frac{2}{\sqrt{\pi}}\int_x^{\infty}\exp(-t^2)dt .$$

The ratio d/l does not appear in V_3^0 since the calculation of this matrix element does not involve particles in different layers. V_0^1 and V_3^0 cross at $d/l = 3.10$ which for $\nu = \frac{1}{5}$ corresponds to $d/a = 0.55$, in good agreement with the boundary in Fig. 1.

It is important to realize that the Fermi statistics and the restriction to the lowest Landau level very severely restrict the form of the wave functions. Apart from the exponential factor, we must have a homogeneous polynomial of degree N in the $z_{i\alpha}$, where N is the degeneracy of the Landau level. Furthermore, the polynomial must be antisymmetric in the $z_{i\alpha}, z_{j\alpha}$. A low energy for $|1,3,1\rangle$ is guaranteed by the fact that it avoids the interlayer $m = 0$ repulsion and the intralayer $m = 1$ repulsion, which are the strongest interactions at small d. Yoshioka *et al.*[13] have already shown numerically that the Jastrow forms are very accurate for the two-layer case.

The pair correlation functions are defined as

$$g(|z_{1\alpha}-z_{2\alpha}|) = \frac{N(N-1)}{\rho^2} \times \frac{\int\cdots\int |\langle 1,s,1\rangle|^2 \prod_{j,\sigma}{}' dz_{j\sigma}}{\langle 1,s,1|1,s,1\rangle} \quad (2.4)$$

for the pairs in the same layer, where $\prod'$ indicates the restricted product for $1 \leq j \leq N$ and $1 \leq \alpha \leq M$ excluding the two terms with $(j,\sigma) = (1,\alpha),(2,\alpha)$.

For the pairs which are γ layers apart, where $\gamma = 1,2,3,\ldots$,

$$f_{\gamma}(|z_{1\alpha}-z_{1,\alpha+\gamma}|) = \frac{N^2}{\rho^2} \times \frac{\int\cdots\int |\langle 1,s,1\rangle|^2 \prod_{j,\sigma}{}'' dz_{j\sigma}}{\langle 1,s,1|1,s,1\rangle} , \quad (2.5)$$

where $\prod''$ means the restricted product for $1 \leq j \leq N$ and $1 \leq \alpha \leq M$ excluding the terms with $(j,\sigma) = (1,\alpha),(1,\alpha+\gamma)$.

The total Coulomb energy per electron is given by

$$u = \frac{e^2}{2MN}\sum_{\substack{1\leq\alpha,\beta\leq M,\\ 1\leq i,j\leq N\\ [(i,\alpha)\neq(j,\beta)]}} \frac{\left\langle 1,s,1\left|\frac{1}{|z_{i\alpha}-z_{j\beta}|}\right|1,s,1\right\rangle}{\langle 1,s,1|1,s,1\rangle} - \frac{e^2\rho}{2}\sum_{\alpha=1}^{M}\int\frac{dz}{(|z|^2+\alpha^2d^2)^{1/2}} . \quad (2.6)$$

The first term is the Coulomb energy between all the electrons and the second term comes from the interaction with a positive neutralizing background. We assume here the location of the background layers coincides with that of 2D EG layers.

We have calculated the pair correlation functions and the Coulomb energies by using Monte Carlo simulations. One can evaluate the energy by integrating the pair correlation functions as shown below:

$$u = \frac{e^2}{2}\rho\int dz\frac{[g(|z|)-1]}{|z|} + \frac{e^2}{2}\rho\sum_{\beta}\int dz\frac{[f_{\beta}(|z|)-1]}{(|z|^2+\beta^2d^2)^{1/2}} , \quad (2.7)$$

where β runs over the nonzero integers $\pm1,\pm2,\ldots$.

We found that the best method was to directly calculate the energy during the simulation. That is, for each configuration generated, we evaluate the Coulomb energy as well as the pair correlation functions and then average over the configurations. We used a system of six layers with periodic boundary conditions in the third direction. Each layer contains 32 particles. When the two-dimensional disk geometry was used, the edge effects were quite large. In order to minimize the edge effects, we mapped the two dimensions in the plane onto a sphere as described by Haldane.[14] We developed at least 7×10^5 configurations in a single run to compute the various properties of the liquid states. The Coulomb energies we obtained are listed in Table I.

As the interlayer separation d is decreased, the uncorrelated Laughlin liquid state $|0,5,0\rangle$ gives way to $|1,3,1\rangle$ at $\frac{1}{5}$ filling. The energies of these two states become equal at $d/a \sim 0.5$. We found it necessary to calcu-

late both energies in the same system to determine the phase boundary accurately. Finite size effects are fairly important at the scale of these energy differences, as already pointed out by other authors.[15] A similar calculation at $\nu=\frac{1}{7}$ shows that the state $|0,7,0\rangle$ changes to $|1,5,1\rangle$ first and then to $|1,1,3,1,1\rangle$, as the interlayer correlation becomes more and more important.

Notice that at $\frac{1}{3}$ filling, we do not have a state like $|1,1,1\rangle$. It turns out that this state is not liquidlike. When Monte Carlo calculations are done in this state, the electron density is not uniformly distributed, as it would be in a liquid state. We will comment on this point again later when we discuss the quasihole excitation in Sec. V.

III. GROUND-STATE ENERGY OF THE SOLID PHASES

We consider a system of electrons centered at three-dimensional lattice sites, with two-dimensional fluctuations in the layer. We found that the phase boundaries are sensitive to the correlations between electron fluctuations at different lattice sites. Therefore we adopted the method of Lam and Girvin[3] to include these correlations.

The variational wave function for a correlated Wigner crystal is expressed as

$$\Psi^c[z_{i\alpha}]=\exp\left[\frac{1}{4}\sum_{\substack{1\le i,j\le N,\\ 1\le\alpha\le M}}(\xi_{i\alpha}B_{ij}\xi_{j\alpha})\right]\times\left[\prod_{\substack{1\le i\le N,\\ 1\le\alpha\le M}}\phi_{R_{i\alpha}}(z_{i\alpha})\right], \tag{3.1}$$

with

$$\phi_{R_{i\alpha}}(z_{i\alpha})=(2\pi)^{-1/2}\exp[-\tfrac{1}{4}(z_{i\alpha}-R_{i\alpha})^2-\tfrac{1}{4}(z^*_{i\alpha}R_{i\alpha}-z_{i\alpha}R^*_{i\alpha})], \tag{3.2}$$

where $z_{i\alpha}=x_{i\alpha}+iy_{i\alpha}$ is the complex expression of the position of the ith electron in the αth layer. $R_{i\alpha}$ are lattice sites, $\xi_{i\alpha}=z_{i\alpha}-R_{i\alpha}$ is the fluctuation away from the ith site in the αth layer. B_{ij} is a complex variational parameter determining the correlation between $\xi_{i\alpha}$ and $\xi_{j\alpha}$.

Within the harmonic approximation, the optimal $B_{\mathbf{k}}$ which is the Fourier transform of B_{ij} is given by

$$B_{\mathbf{k}}=\frac{\omega_L(\mathbf{k})-\omega_T(\mathbf{k})}{\omega_L(\mathbf{k})+\omega_T(\mathbf{k})}\exp(-i\theta_{\mathbf{k}}), \tag{3.3}$$

where $\omega_L(\mathbf{k})$ and $\omega_T(\mathbf{k})$ are the longitudinal and transverse classical phonon frequencies, respectively. $\theta_{\mathbf{k}}$ is a phase related to the classical dynamical matrix.[3]

The total phonon energy is

$$E=\frac{m_e^*l^2}{2}\sum_{\mathbf{k}}\tfrac{1}{2}[\omega_L(\mathbf{k})+\omega_T(\mathbf{k})]^2 \le\frac{m_e^*l^2}{2}\sum_{\mathbf{k}}[\omega_L^2(\mathbf{k})+\omega_T^2(\mathbf{k})], \tag{3.4}$$

where m_e^* is the effective electron mass. The energy is lowered from the uncorrelated case [the second line of

TABLE I. Coulomb energies per electron of the liquid states in units of $e^2/\epsilon l$. The energies of states $|0,m,0\rangle$ calculated by Levesque *et al.* (Ref. 26) are $u(|0,5,0\rangle)=-0.3277\pm0.0002$, $u(|0,7,0\rangle)=-0.2810\pm0.0002$, and from the extrapolation formula given there, $u(|0,9,0\rangle)=-0.2495\pm0.0002$.

d/a	$u(\|1,3,1\rangle)$	$u(\|0,5,0\rangle)$	$u(\|1,1,3,1,1\rangle)$	$u(\|1,5,1\rangle)$	$u(\|0,7,0\rangle)$	$u(\|1,7,1\rangle)$	$u(\|0,9,0\rangle)$
0.2	−0.377±0.002		−0.326±0.002	−0.322±0.002		−0.288±0.001	
0.3	−0.354±0.001		−0.299±0.002	−0.303±0.002		−0.272±0.001	
0.4	−0.339±0.001		−0.284±0.002	−0.293±0.001		−0.263±0.001	
0.5	−0.331±0.001	−0.3334±0.0004	−0.275±0.002	−0.287±0.001		−0.258±0.001	
0.6	−0.325±0.002		−0.270±0.003	−0.283±0.001	−0.2856±0.0004	−0.255±0.001	
0.7	−0.321±0.002		−0.267±0.003	−0.281±0.001		−0.253±0.001	−0.2537±0.0005
0.8	−0.319±0.002		−0.265±0.003	−0.280±0.001		−0.252±0.001	

TABLE II. The coefficients $a_{1/2}$, $a_{3/2}$, and $a_{5/2}$ in Eq. (2.12).

d/a	$a_{1/2}$	$a_{3/2}$	$a_{5/2}$	Lattice structure
0.5	−0.830 3649	0.5046	0.33	bct
0.7	−0.795 0830	0.3768	0.25	bct
0.8	−0.787 4528	0.3392	0.22	bct
0.9	−0.784 6556	0.3202	0.21	hcp
1.0	−0.783 4247	0.3045	0.20	hcp
1.2	−0.782 4698	0.2837	0.19	hcp
1.5	−0.782 1774	0.2523	0.17	hcp
∞ (single layer)	−0.782 133	0.2410	0.16	2D triangular lattice

Eq. (3.4)] by favoring the fluctuations with less energy (the transverse mode) and disfavoring the fluctuations with more energy (the longitudinal mode).

We have calculated the Coulomb energy for both the hexagonal-close-packed (hcp) and the body-centered-tetragonal (bct) lattices at various separation d. The energy per electron can be fitted to the following form:

$$u = a_{1/2}\nu^{1/2} + a_{3/2}\nu^{3/2} + a_{5/2}\nu^{5/2} , \tag{3.5}$$

where the coefficients $a_{1/2}$, $a_{3/2}$, and $a_{5/2}$ are listed in Table II.

The first term is the classical energy corresponding to the point charge lattice. The second term comes from the harmonic expansion of the Coulomb potential, i.e., the phonon energy given by Eq. (3.4). The last term corresponds to the quartic expansion of the Coulomb potential and the coefficient was obtained by interpolating the result of Lam and Girvin[3] for the triangular lattice.

We know that in two-dimensional space, the triangular lattice has the lowest energy. Consistent with this we found that the hcp structure is the three-dimensional ground state at large separation d. As d decreases, the repulsion between the electrons in neighboring layers plays a more important role. At $d/a < 0.9$, the point charge energy [i.e., the first term in Eq. (3.5)] of the bct structure is lower than that of hcp. At this point the phonons in the hcp structure start to show soft modes, as shown in Table III. The negative $\omega_T^2(\mathbf{k})$ indicates the state is no longer stable. The frequencies are calculated without including the magentic field. It can be shown that the inclusion of the field would not change the stability boundary at all.

When d is decreased further, the bct lattice becomes unstable at $d/a < 0.5$ where we see soft phonon modes. When the layers are very close to each other, the interaction between the electron pairs directly above each other, i.e., with the same lateral coordinates, dominates the Coulomb energy. In the bct structure, these pairs are two layers apart. For small d, this configuration must give way to structures with a longer period in the third direction or even an incommensurate structure. We tried some of these structures, and they did indeed have lower energies than the bct lattice, as shown in Table IV.

Here we explain the optimal structures shown in Table IV. They are regarded as a stack of square lattice layers at distance d apart. For periodic stacking with period n in the third direction, we keep the zeroth and the nth layer directly above each other. Then shift the $n-1$ layers in between until we get a set of two-dimensional displacements relative to the zeroth layer, which minimizes the energy. For $n=2$, the optimal displacement of the first layer we got was $\Delta_1=(0.5,0.5)a$. This is just the bct lattice. For $n=4$, $\Delta_1=(0.5,0.5)a$, $\Delta_2=(0,0.5)a$, $\Delta_3=(0.5,0)a$. For $n=5$, $\Delta_1=(0.39,0.21)a$, $\Delta_2=(0.60,0.81)a$, $\Delta_3=(0.20,0.61)a$, $\Delta_4=(0.79,0.40)a$. For nonperiodic stacking, the optimal displacements listed in Table IV are obtained under the assumption that each layer is shifted by the same amount relative to the previous one. The value of Δ's in the table measures this relative displacement. Among this class of states, we do see the trend toward longer periods as d is reduced. But even for the lowest-energy states of this form there are soft phonon modes. The true ground state at very small separation is still unknown.

This suggests that one must consider the possibility of a staging transition. As suggested in Ref. 9, staging transitions in multiple-quantum-well system might occur at $d^3\bar{\rho} \leq 0.3$ (where $\bar{\rho}=\rho/d$ is the three-dimensional electron density), which corresponds to $d/a=(d^3\bar{\rho})^{1/2} \leq 0.55$. This result was based on a simple model calculation in which the influence of the Wigner crystallization in a 2D EG layer on the interlayer interaction was ignored. The Madelung energy of a two-dimensional triangular lattice[16] was used to approximate the exchange and correlation energy within a layer.

We have done a refined calculation by considering a stack of 2D EG layers in a bct arrangement, since we have found that the bct structure has lower energy than

TABLE III. Phonon modes of the bct and hcp lattices. A minus sign indicates a soft mode.

	sgn[$\omega^2(k)$]	
d/a	bct	hcp
<0.4	−	−
0.5–0.8	+	−
>0.9	−	+

TABLE IV. Comparison of classical Coulomb energies of the bct structure and the energy of the corresponding optimal structure, denoted by $^*u$. The optimal structures are described in the text.

d/a	$u_{\rm bct}$ $(\nu^{1/2}e^2/\epsilon l)$	$^*u$ $(\nu^{1/2}e^2/\epsilon l)$	Optimal structure
0.1	−0.347 2234	−1.251 5810	$n=5$
0.2	−0.896 3031	−1.011 2565	$n=4$
0.3	−0.903 3237	−0.923 5738	Inc. $\Delta=(0.344,0.500)$
0.4	−0.863 7858	−0.865 5102	Inc. $\Delta=(0.400,0.500)$
0.5	−0.830 3649	−0.830 3649	$n=2$ (bct)

hcp at small d. The total Coulomb energy was calculated by carrying out the lattice summation using an Ewald transformation. This calculation leads to a reduced critical density for staging transitions: $d^3\bar{\rho}\leq 0.09$, i.e., $d/a\leq 0.3$. The energies of stage-n states with the lowest energy at various d/a are listed in Table V along with the energies of $n=1$ state for comparison. (ν is the filling factor in a $n=1$ state of the same density $\bar{\rho}$.)

Based on the information given in Secs. II and III, we have constructed the zero-temperature phase diagram as a function of the Landau filling factor ν and the interlayer separation d, as shown in Fig. 1.

IV. PAIR CORRELATION FUNCTIONS OF THE LIQUIDLIKE GROUND STATES

By using Monte Carlo simulations, we have computed the pair correlation functions of the various liquid states. The pair correlation functions for states $|1,5,1\rangle$ and $|1,1,3,1,1\rangle$ at $\nu=\frac{1}{7}$ are shown in Figs. 2 and 3. The results of the analogous calculation for the $|1,3,1\rangle$ state have been published previously.[6]

In state $|1,5,1\rangle$, we can see that the correlation functions for the same layer and next layer have the same shape as in Laughlin states, while the functions for the second-neighbor and third-neighbor layers show some three-dimensional solidlike correlations at small r. They do not vanish at $r=0$ but show a large probability there. This is similar to the bct arrangement. The electrons in adjacent layers try to avoid having the same in-plane coordinates. Thus the best way for an electron in the first layer is to occupy the spot halfway between the electrons in the zeroth layer. Electrons in the second layer then have a high probability of being directly above electrons in the zeroth layer.

For the $|1,1,3,1,1\rangle$ state, the correlation functions for pairs in next layer and second-neighbor layer are similar, since the wave function includes the same interlayer correlation for these pairs. Therefore we did not draw the line for the second-neighbor layer; it is indicated by points on the curve for the next layer instead. The correlation function for second-neighbor layers does not show the peak at $r=0$ that occurs in the $|1,5,1\rangle$ state. (It is prevented by the correlation terms which appear in the second type of wave function.) This effect is analogous to the period lengthening at small d which we found above for the solid states.

At long lateral separations, the correlation functions show the usual damped oscillations characteristic of a liquid. Note that the oscillations in neighboring layers are 180° out of phase for the $|1,5,1\rangle$ state reflecting the attempts of the particles to avoid each other.

TABLE V. Classical Coulomb energies of stage-n states in units of $e^2/\epsilon l$. The calculation method is described in the text.

d/a	Stage n	u_n $(\nu^{1/2}e^2/\epsilon l)$	u_1 $(\nu^{1/2}e^2/\epsilon l)$
<0.1	4,5,6,. . .		
0.1	3	−1.262 173 6	−0.347 223 4
0.2	2	−1.026 882 1	−0.896 303 1
0.3	2	−0.922 248 8	−0.903 323 7
0.4	1	−0.863 785 8	−0.863 785 8
>0.4	1		

V. QUASIPARTICLE EXCITATIONS OF THE LIQUID STATES

Now we turn to the excitation properties of the liquid states. Let us first look at the simplest quasihole excitation one can construct by analogy to the two-dimensional situation. For ground state $|1,s,1\rangle$ at $1/(s+2)$ filling, we get

$$|1,s,1;z_0\rangle=\left[\prod_{i=1}^{N}(z_{i0}-z_0)\right]|1,s,1\rangle\ , \tag{5.1}$$

where z_0 is a fixed c-number. We can apply the screening argument for the equivalent classical multicomponent

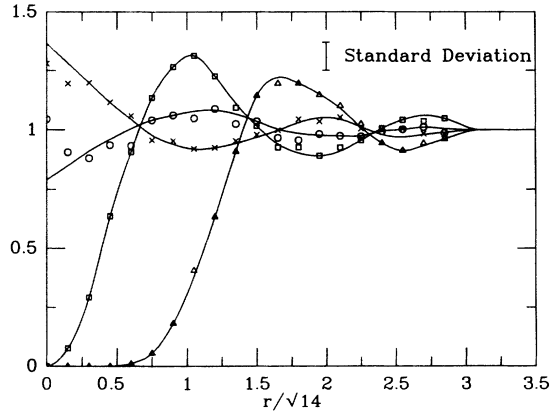

FIG. 2. Pair correlation functions for electrons in the $|1,5,1\rangle$ state, calculated numerically. Correlations are shown for particles in the same layer (△), next layer (□), second-neighbor layer (×), and third-neighbor layer (○).

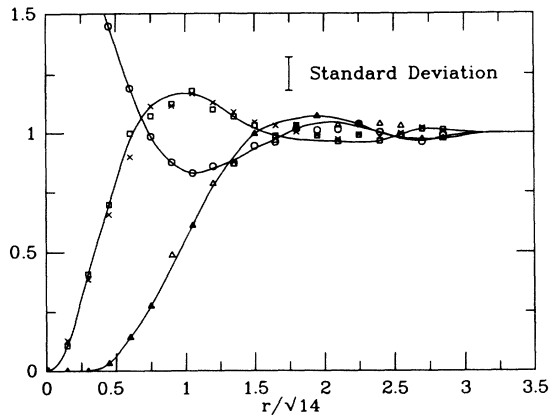

FIG. 3. Pair correlation functions for electrons in the $|1,1,3,1,1\rangle$ state, calculated numerically. Correlations are shown for particles in the same layer (△), next layer (□), second-neighbor layer (×), and third-neighbor layer (○).

plasma to obtain the charge on the excitation. Recall that the plasma consists of M types of particles interacting pairwise with logarithmic interactions. The coupling constant for each pair is determined by the layer separation. If the particles are the same type, i.e., they belong to the same layer, the coupling is proportional to s. If they belong to neighboring layers, the coupling is unity. Particles in more distant layers do not interact.

The wave function $|1,s,1;z_0\rangle$ corresponds to a plasma system with a phantom plasma "charge" 1 at z_0 in the zeroth layer. The particles in the same layer of "charge" s and the particles in the neighboring layers 1 and -1 of "charge" 1 will accumulate an equal and opposite "charge" around the phantom to completely screen it. Therefore the screening charges (the real electric charges) in layer $-1,0,1$ satisfy the condition $sq_0+q_1+q_{-1}=e$. There is no phantom in the ith layer when $i\neq 0$, and so we have $sq_i+q_{i+1}+q_{i-1}=0$.

We can write these screening equations in a matrix form:

$$\sum_j A_{ij}q_j=e\delta_{i,0} , \tag{5.2}$$

where

$$A_{ij}=s\delta_{i,j}+\delta_{i,j+1}+\delta_{i,j-1} .$$

Summing Eq. (5.2) over i, we get the total charge on the excitation:

$$\sum_j q_j=\frac{e}{s+2}=\nu e , \tag{5.3}$$

which is the same as it would be in state $|0,s+2,0\rangle$. Thus a transition at constant density does not change the *total* charge on the quasiparticle, nor will it change the quantized Hall conductance.

The screening charge in each layer can be obtained by Fourier transformation of Eq. (5.2). We define the quantities

$$q_n=\frac{1}{2\pi}\int_{-\pi}^{\pi}e^{ikn}q_k dk \quad \text{with} \quad q_k=\sum_{n=-\infty}^{\infty}e^{-ikn}q_n , \tag{5.4}$$

$$A_n=\frac{1}{2\pi}\int_{-\pi}^{\pi}e^{ikn}A_k dk \quad \text{with} \quad A_k=\sum_{n=-\infty}^{\infty}e^{-ikn}A_n . \tag{5.5}$$

Then Eq. (5.2) becomes $A_k q_k=1$. Therefore $q_k=1/A_k$.

For a state $|1,s,1\rangle$, $A_k=s+2\cos k$; then

$$q_n=\frac{1}{2\pi}\int_{-\pi}^{\pi}\frac{e^{ikn}}{s+2\cos k}dk=\frac{\lambda^{|n|}}{(s^2-4)^{1/2}} , \tag{5.6}$$

where $\lambda=[-s+(s^2-4)^{1/2}]/2$. The charge q_n has an oscillatory behavior since λ is a negative number. $q_0=e/(s^2-4)^{1/2}$ is larger than the value for $|0,s,0\rangle$ ($q_0=e/s$). It indicates that the zeroth layer is over screened. More spectacular is that this charge is an irrational fraction of the electron charge. It is observable in principle since the charge densities in different layers are spatially separated.

We also directly simulated the behavior of the quasihole state in order to compare with Eq. (5.6). The electron density of each layer in the $|1,3,1;z_0\rangle$ state is plotted in Fig. 4.

The screening charge in each layer can be obtained by integrating the charge densities over a region of size $\sim l$:

$$q_n=\int[\rho_g-\rho_n(z)]dz , \tag{5.7}$$

where $\rho_g=\frac{1}{10}\pi l^2$ is the uniform density of the ground state $|1,3,1\rangle$ and $\rho_n(z)$ is the charge density of the nth layer in $|1,3,1;z_0\rangle$ state.

In order to compare the q_n's from the simulation with the q_n's from the screening argument, we have solved Eq. (5.2) for a system of six layers which is the system we simulated by Monte Carlo techniques. Both the solution of Eq. (5.2) and the Monte Carlo results are listed in Table VI. For a system with finite number of layers, the q_n's are rational.

Now let us turn back to the stability condition of the

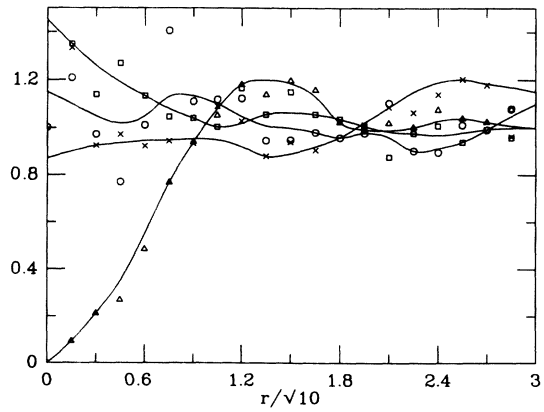

FIG. 4. Electron density of each layer in the $|1,3,1;z_0\rangle$ state. Shown in the figure are electron density of the layer with the quasihole (△), next layer (□), second-neighbor layer (×), and third-neighbor layer (○).

TABLE VI. Screening charges in the $|1,3,1;z_0\rangle$ state. The first two columns of q_n's are the solutions of Eq. (5.2).

Layer n	q_n (∞ layers)	q_n (six layers)	q_n (six layers, Monte Carlo)
0	0.447	0.450	0.38±0.06
1	−0.171	−0.175	−0.14±0.06
2	0.065	0.075	0.06±0.06
3	−0.025	−0.050	−0.04±0.06
4	0.010	0.075	0.06±0.06
5	−0.004	−0.175	−0.14±0.06

liquid states. The A_k's in Eq. (5.5) can be interpreted as the 2D spatially averaged static dielectric function of the plasma.

The dielectric function is defined by

$$\phi^{\text{ext}}(\mathbf{r}_\perp,n)=\sum_{n'}\int d^2\mathbf{r}'_\perp\,\epsilon(\mathbf{r}_\perp,\mathbf{r}'_\perp,n,n')\phi(\mathbf{r}'_\perp,n')\ , \tag{5.8}$$

with $\mathbf{r}_\perp,\mathbf{r}'_\perp\perp\hat{\mathbf{z}}$, and n,n' are indices of layers. Here ϕ^{ext} is the external potential and ϕ is the total potential. Its Fourier transform is defined by

$$\epsilon(\mathbf{p}_\perp,k)=\sum_n\int d^2\mathbf{r}_\perp\exp(-i\mathbf{p}_\perp\cdot\mathbf{r}_\perp)\exp(-ikn)\epsilon(\mathbf{r}_\perp,n) \tag{5.9}$$

It is then straightforward to show that ϵ is related to A_k by

$$\epsilon(\mathbf{p}_\perp=\mathbf{0},k)=\frac{A_k}{A_k-1}\ . \tag{5.10}$$

For example, the state $|\beta,\alpha,\beta\rangle$ has a screening matrix $A_{ij}=\alpha\delta_{ij}+\beta\delta_{i,j-1}+\beta\delta_{i,j+1}$, with

$$A_k=\sum_{i-j=-\infty}A_{i-j}\exp ik(i-j)=\alpha+2\beta\cos k\ . \tag{5.11}$$

Considering the $|1,1,1\rangle$ state, we get $A_k=0$ for $k=\pm 2\pi/3$. This indicates instability toward a charge density wave with modulation perpendicular to the layers. We see later that a soft mode occurs when $A_k=0$.

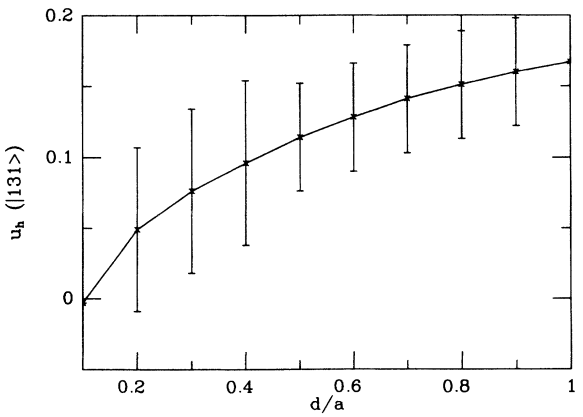

FIG. 5. The excitation energy for a quasihole in the $|1,3,1;z_0\rangle$ state, in units of $e^2/\epsilon l$.

A liquid state is stable if $A_k>0$ for all k, as is the case for states $|1,3,1\rangle$ and $|1,5,1\rangle$. However, the state $|1,1,1\rangle$ is not stable, as verified by our Monte Carlo results. For a state $|\gamma,\beta,\alpha,\beta,\gamma\rangle$, $A_k=\alpha+2\beta\cos k+2\gamma\cos 2k$. For example, for $|1,1,3,1,1\rangle$, we have $A_k=3+2\cos k+2\cos 2k$, which is always positive.

We also calculated the energy difference between the state $|1,3,1;z_0\rangle$ and $|1,3,1\rangle$ at various separations d using Monte Carlo simulations. The quasihole energy u_h we obtained is plotted in Fig. 5 as a function of d. u_h in this correlated state is around $0.1e^2/\epsilon l$, much larger than that of the state $|0,5,0\rangle$ (which is $0.007e^2/\epsilon l$). The reason for the large difference in the excitation energies may be understood if one recalls that this energy is proportional to the square of the quasiparticle charge in the 2D case. In the 3D case, a reasonable first approximation is that the energy should be the sum of the squares of the charges in the different layers. Because of overscreening, therefore, the energy in $|1,3,1\rangle$ will be much greater than in $|0,5,0\rangle$. Because this energy determines the size of the cusp in the energy versus density relation, we expect that the stability region for the $|1,3,1\rangle$ state will be wide. The difference in excitation energies should be very helpful to the experimental observation of the liquid-liquid transition at constant electron density, since these two liquid states have very different activation energies for thermodynamic and transport properties.

VI. COLLECTIVE EXCITATIONS OF THE LIQUID STATES: AN OVERVIEW

A single 2D EG layer with an incompressible ground state has a branch of intra-Landau-level collective modes, known as magnetorotons. The existence of these modes was first proposed by Girvin *et al.*,[17] who evaluated their dispersion relation by using a single-mode approximation (SMA) in which the magnetoroton was assumed to exhaust all the oscillator strength available to intra-Landau-level excitations. The SMA, which has been shown to be extremely accurate[14] except in the short-wavelength limit, is equivalent to approximating the unnormalized magnetoroton wave function by

$$|\Psi_{\mathbf{k}_\perp}\rangle=\bar{\rho}(\mathbf{k}_\perp)|\Psi_0\rangle\ , \tag{6.1}$$

where $|\Psi_0\rangle$ is the incompressible ground state, $\bar{\rho}(\mathbf{k}_\perp)$ is the density operator projected onto the lowest Landau level, and $\mathbf{k}_\perp$ is a 2D wave vector. For a multilayer system, magnetorotons can be created in each layer and will

couple to form a magnetoroton band. These bands have been discussed previously[18] using an approach in which interlayer correlations are treated in a random-phase approximation. This approach is expected to be accurate when interlayer correlations are weak and is not applicable to the present case, where the incompressible state is itself based on strong-interlayer correlations and specifically on the exclusion of some low interlayer relative-angular-momentum channels. To make progress here we must generalize the SMA to the multilayer case. We find that the SMA excitation energies can be expressed in terms of the intralayer and interlayer correlation energies discussed previously. Moreover, the occurrence of a gap in the long-wavelength limit, necessary for dissipationless transport, depends on sum rules obeyed by the correlation functions of the incompressible state. These sum rules reflect the same screening properties as those which determine the quasiparticle charges.

VII. SMA EXCITATION ENERGIES

The unnormalized wave function for a state with a magnetoroton with 2D wave vector $\mathbf{k}_\perp$ in layer α is

$$|\Psi_\alpha(\mathbf{k}_\perp)\rangle=\bar{\rho}_\alpha(\mathbf{k}_\perp)|\Psi_0\rangle=\sum_{i=1}^{N}B_{i\alpha}(\mathbf{k}_\perp)|\Psi_0\rangle\ , \tag{7.1}$$

where

$$B_{i\alpha}(\mathbf{k}_\perp)=\overline{\exp(-i\mathbf{k}_\perp\cdot\mathbf{r}_{\perp i\alpha})} \tag{7.2}$$

is the projection of $\exp(-i\mathbf{k}_\perp\cdot\mathbf{r}_{\perp i\alpha})$ onto the lowest Landau level and $\mathbf{r}_{\perp i\alpha}$ is the 2D coordinate of an electron in layer α. To normalize the wave functions we need to evaluate

$$\begin{aligned}\langle\Psi_{\alpha'}(\mathbf{k}_\perp)|\Psi_\alpha(\mathbf{k}_\perp)\rangle&=N[\delta_{\alpha',\alpha}\exp(-|\mathbf{k}_\perp|^2/2)+h_{\alpha',\alpha}(\mathbf{k}_\perp)]\\&\equiv N\bar{S}_{\alpha',\alpha}(k)\ .\end{aligned} \tag{7.3}$$

Equation (7.3) follows from the identity[19]

$$B_{i\alpha}(\mathbf{k}_{1\perp})B_{i\alpha}(\mathbf{k}_{2\perp})=\exp(k_1^*k_2/2)B_{i\alpha}(\mathbf{k}_{1\perp}+\mathbf{k}_{2\perp})\ . \tag{7.4}$$

(In this section, we set $l=1$.) In Eq. (7.4), $k_i=k_{x_i}+ik_{y_i}$ is the 2D wave vector expressed as a complex number,

$$h_{\alpha',\alpha}(k)=\rho\int d\mathbf{r}\exp(-i\mathbf{k}\cdot\mathbf{r})h_{\alpha',\alpha}(\mathbf{r}-\mathbf{r}')\ , \tag{7.5}$$

and the pair correlation function

$$\begin{aligned}h_{\alpha',\alpha}(\mathbf{r}-\mathbf{r}')&=\rho^2\langle\Psi_0|\sum_{1\le i,j\le N}{}'\delta(\mathbf{r}-\mathbf{r}_{i\alpha'})\delta(\mathbf{r}'-\mathbf{r}_{j\alpha})|\Psi_0\rangle-1\\&=g(\mathbf{r}-\mathbf{r}')-1\ .\end{aligned} \tag{7.6}$$

The prime on the sum in Eq. (7.6) indicates that $i=j$ is excluded if $\alpha'=\alpha$.

We see from the above that magnetorotons in different layers are not orthogonal. Moreover, they will be coupled through the Coulomb interaction. We therefore exploit the invariance of the ground state and the Hamiltonian under translation by an integral number of layers and define

$$|\Psi(\mathbf{k}_\perp,k_z)\rangle\equiv|\Psi(\mathbf{k})\rangle=\frac{1}{\sqrt{M}}\sum_{\alpha=1}^{M}\exp(ik_zZ_\alpha)|\Psi_\alpha(\mathbf{k}_\perp)\rangle\ . \tag{7.7}$$

In Eq. (7.7), M is again the number of layers in the system, which will be taken to infinity, and Z_α is the z coordinate of the αth layer.

Using Eq. (7.3) we see that

$$\langle\Psi(\mathbf{k}')|\Psi(\mathbf{k})\rangle=\delta_{\mathbf{k},\mathbf{k}'}N\bar{S}(\mathbf{k})\ , \tag{7.8}$$

where

$$\bar{S}(\mathbf{k})=\bar{S}(\mathbf{k}_\perp,k_z)=\sum_{\alpha=1}^{M}\exp(-ik_zZ_\alpha)\bar{S}_{0\alpha}(\mathbf{k}_\perp)\ . \tag{7.9}$$

The SMA for the collective excitation dispersion is obtained by evaluating

$$\begin{aligned}\frac{\langle\Psi(\mathbf{k})|H|\Psi(\mathbf{k})\rangle}{\langle\Psi(\mathbf{k})|\Psi(\mathbf{k})\rangle}&=E_0+\frac{\langle\Psi_0|[\bar{\rho}(-\mathbf{k}),[H,\bar{\rho}(\mathbf{k})]]|\Psi_0\rangle}{2MN\bar{S}(\mathbf{k})}\\&\equiv E_0+\Delta(\mathbf{k})\ .\end{aligned} \tag{7.10}$$

In Eq. (7.10), E_0 is the ground-state energy and $\Delta(\mathbf{k})$ is the excitation energy, and

$$\begin{aligned}\bar{\rho}(\mathbf{k})\equiv\bar{\rho}(\mathbf{k}_\perp,k_z)&=\sum_{\alpha=1}^{M}\exp(-ik_zZ_\alpha)\bar{\rho}_\alpha(\mathbf{k}_\perp)\\&=\sum_{\substack{1\le i\le N,\\1\le\alpha\le M}}\exp(-ik_zZ_\alpha)B_{i\alpha}(\mathbf{k}_\perp)\ .\end{aligned} \tag{7.11}$$

The double commutator may be evaluated by writing

$$H=\int\frac{d^2\mathbf{q}_\perp}{(2\pi)^2}\int_{-\pi}^{\pi}\frac{dq_z}{2\pi}\frac{2\pi e^2}{q_\perp}S(\mathbf{q})\bar{\rho}(-\mathbf{q})\bar{\rho}(\mathbf{q})+\text{const}\ , \tag{7.12}$$

where we use the layer separation d as the length unit in the z direction and

$$S(\mathbf{q})=S(\mathbf{q}_\perp,q_z)=\frac{\sinh(q_\perp d)}{\cosh(q_\perp d)-\cos q_z}\ . \tag{7.13}$$

Using Eq. (7.4) we find that

$$\Delta(\mathbf{k})=\int_{-\pi}^{\pi}\frac{dq_z}{2\pi}\int\frac{d^2\mathbf{q}_\perp}{(2\pi)^2}\exp(-|\mathbf{q}_\perp|^2/2)\frac{2\pi e^2}{q_\perp}S(\mathbf{q})[1-\cos(k_\perp q_\perp\sin\theta)]\frac{\bar{S}^{\sim}(\mathbf{k}+\mathbf{q})-\bar{S}^{\sim}(\mathbf{q})}{\bar{S}^{\sim}(\mathbf{k})}\ , \tag{7.14}$$

where $\bar{S}^{\sim}(\mathbf{p})=\exp(|\mathbf{p}|^2/2)\bar{S}(\mathbf{p})$ and θ is the angle between $\mathbf{k}$ and $\mathbf{q}$. If the ground state is a $|0,m,0\rangle$ state, i.e., it has no interlayer correlations, $\bar{S}^{\sim}(\mathbf{p})$ becomes independent of p_z [see Eqs. (7.9) and (7.3)] and the integral over q_z in Eq. (7.14) may be performed to yield

$$\Delta(\mathbf{k}_\perp,k_z)=\Delta_{2D}(\mathbf{k}_\perp)=\int\frac{d^2\mathbf{q}_\perp}{(2\pi)^2}\exp(-|\mathbf{q}_\perp|^2/2)\frac{2\pi e^2}{q_\perp}[1-\cos(k_\perp q_\perp\sin\theta)]\frac{\bar{S}^{\sim}(\mathbf{k}+\mathbf{q})-\bar{S}^{\sim}(\mathbf{q})}{\bar{S}^{\sim}(\mathbf{k}_\perp)}\ . \tag{7.15}$$

Thus the result for an isolated 2D layer is recovered. In the presence of interlayer correlations $\Delta(\mathbf{k})$ becomes dependent on k_z.

It is important to examine the expression for $\Delta(\mathbf{k})$ to ensure that the excitation gap required for dissipationless transport is maintained at long wavelengths. We first examine the case where $\mathbf{k}_\perp$ approaches zero and k_z is not equal to zero. In this regime,

$$\Delta(\mathbf{k})\sim\frac{k_\perp^2}{4}\int_{-\pi}^{\pi}dq_z\int\frac{d^2\mathbf{q}_\perp}{(2\pi)^2}\exp(-|\mathbf{q}_\perp|^2/2)q_\perp^2S(\mathbf{q})\left[\frac{\bar{S}^{\sim}(\mathbf{q}_\perp,q_z+k_z)-\bar{S}^{\sim}(\mathbf{q}_\perp,q_z)}{\bar{S}^{\sim}(\mathbf{k})}\right], \tag{7.16}$$

which goes as $k_\perp^2/\bar{S}^{\sim}(\mathbf{k}_\perp,k_z)$. For $k_z=0$, the numerator of the term in large parentheses in Eq. (7.16) vanishes and $\Delta(\mathbf{k}_\perp)$ goes like $k_\perp^4/\bar{S}^{\sim}(\mathbf{k}_\perp,k_z=0)$ at long wavelength. Clearly the existence of an excitation gap depends on how $\bar{S}^{\sim}(\mathbf{k}_\perp)$ behaves at long wavelength, which, as we now show, is determined by the screening properties of the corresponding plasma.

VIII. MULTICOMPONENT GENERALIZED PLASMA

For a classical system, the static density-density response function is simply related to pair correlation functions.[20] For the plasma analogue of our multilayer Jastrow wave functions, the charge density induced in layer n when an impurity is introduced which couples only to layer zero particles is

$$\delta\rho_n(k)=-\rho[h_{n0}(k)+\delta_{n,0}]v_0(k)\ , \tag{8.1}$$

where ρ is again the average areal density of particles and $v_0(k)$ is the Fourier transform of the external potential. When the external potential is a charge to which the particles couple with unit strength, i.e., $v_0(k)=4\pi/k^2$, the long range of the interaction guarantees that the coupling strength weighted total induced charge plus impurity charge must vanish for each layer. It follows from Eq. (8.1) then that

$$\lim_{k\to0}\sum_j A_{0,j}\delta\rho_j(k)=\delta_{0,j}\ , \tag{8.2}$$

where $A_{i,j}$ is the screening matrix defined in Eq. (5.2).

Comparing Eqs. (8.2) and (8.1) with Eq. (5.2) we see that

$$\lim_{k\to0}h_{n,0}(k)=-\delta_{n,0}+\frac{k^2}{2}\frac{q_n}{\nu}+\cdots\ . \tag{8.3}$$

For uncoupled layers, $q_n=\nu\delta_{n,0}$ and Eq. (8.3) reduces to the long-wavelength behavior $[h(k)=-1+k^2/2+\cdots]$ responsible for the SMA gap of isolated layers.[17] Equation (8.3) implies the multicomponent generalization of the pair correlation function moment sum rules derived by Forrester and Jancovici[21] for two-component systems. For the multilayer case the sum rules are

$$\int_0^\infty dr\ rh_{n,0}(r)=-\delta_{n,0}/\nu\ , \tag{8.4a}$$

$$\int_0^\infty dr\ r^3h_{n,0}(r)=-q_n/\nu^2\ . \tag{8.4b}$$

Equation (8.3) implies that

$$\begin{aligned}\lim_{k_\perp\to0}\bar{S}(\mathbf{k}_\perp,k_z)&=\sum_n\exp(-i2\pi k_zn)[\lim_{k_\perp\to0}\bar{S}_{0,n}(k_\perp)]\\&=\frac{k_\perp^2}{2}\sum_n\exp(-i2\pi k_zn)\left[-\delta_{n,0}+\frac{q_n}{\nu}\right]\\&=\frac{k_\perp^2}{2}\left[-1+\frac{A(k_z=0)}{A(k_z)}\right].\end{aligned} \tag{8.5}$$

[Note that this is always positive since $A(k_z)<A(k_z=0)$.] Comparing Eq. (8.5) and Eq. (7.16) we see that for k_z not equal to zero,

$$\lim_{k_\perp\to0}\Delta(\mathbf{k}_\perp,k_z)$$

is a constant. For $k_z=0$, $\bar{S}(\mathbf{k}_\perp,k_z)$ vanishes as $k_\perp^4$ so that

$$\lim_{k_\perp\to0}\Delta(\mathbf{k}_\perp,k_z)$$

approaches a different constant. In general, the long-wavelength limit is singular and the gap depends on $(k_z/k_\perp)$.

Comparing Eq. (8.5) and Eq. (7.16) we also see that

$$\lim_{k_\perp\to0}\Delta(\mathbf{k}_\perp,k_z)$$

will vanish whenever $A(k_z)=0$. The vanishing excitation energy is symptomatic of an instability toward CDW states with modulation along the layers,[9] as mentioned previously.

IX. NUMERICAL ESTIMATES

We have estimated the excitation energies of the multilayer Jastrow states using Eq. (7.14) and the Monte Carlo correlation functions discussed previously. Intralayer correlation functions were fitted to the form[17,22]

$$\begin{aligned}h_{00}(r)&=g_{00}(r)-1\\&=-\exp(-r^2/2)-2\sum_l{}'\frac{C_l^{(0)}}{l!}\left[\frac{r^2}{4}\right]^l\exp(-r^2/4)\ .\end{aligned} \tag{9.1}$$

The prime on the sum in Eq. (9.1) indicates that even values of l are excluded from the sum. In Eq. (9.1),

$(1-C_l^{(0)})$ is the ratio of the probability that a pair of electrons will have relative angular momentum l, to the same probability in an uncorrelated state. (Only odd relative angular momentum are allowed within a layer.) Thus, for a Jastrow state which excludes relative angular momentum l, $C_l^{(0)}=1$. The sum rules (8.4a) and (8.4b) require that

$$\sum_l{}' C_l^{(0)}=(\nu^{-1}-1)/4 , \tag{9.2a}$$

$$\sum_l{}' (l+1)C_l^{(0)}=(q_0/\nu^2-1)/8 . \tag{9.2b}$$

Equation (9.1) can be Fourier transformed to yield

$$\bar{S}_{00}(\mathbf{k}_\perp)=(1-\nu)\exp(-|\mathbf{k}_\perp|^2/2) -4\nu\exp(-|\mathbf{k}_\perp|^2)\sum_l{}' C_l^{(0)}L_l(|\mathbf{k}_\perp|^2) , \tag{9.3}$$

where $L_l(x)$ is a Laguerre polynomial.

For interlayer correlation functions even relative angular momentum are not excluded, and we fit to the form

$$h_{0,n}(r)=g_{0,n}(r)-1 =-\sum_{l=0}^{\infty}\frac{C_l^{(n)}}{l!}\left[\frac{r^2}{4}\right]^l\exp(-r^2/4) . \tag{9.4}$$

Again $C_l^{(n)}=1$ if relative angular momentum l between layers 0 and n is excluded. For interlayer correlations the sum rules [Eqs. (8.4a) and (8.4b)] require that

$$\sum_{l=0}^{\infty} C_l^{(n)}=0, \quad n\neq 0 ; \tag{9.5a}$$

$$\sum_{l=0}^{\infty} (l+1)C_l^{(n)}=q_n/4\nu^2, \quad n\neq 0 . \tag{9.5b}$$

Equation (9.4) can be Fourier transformed to yield

$$\bar{S}_{0,n}(\mathbf{k}_\perp)=-2\nu\exp(-|\mathbf{k}_\perp|^2)\sum_{l=0}^{\infty} C_l^{(n)}L_l(|\mathbf{k}_\perp|^2) . \tag{9.6}$$

We have obtained values of $C_l^{(n)}$ by setting $C_l^{(n)}$ to 1 if the corresponding relative angular momentum is excluded from the ground state, and fitting to the Monte Carlo correlation functions while enforcing the sum rule constraints. The sums over relative angular momenta were truncated at the smallest values of l for which a good fit could be obtained, in accord with the expectation that correlations will have little effect on the probability of electrons having a large relative angular momentum. The construction of $\bar{S}(\mathbf{k}_\perp,k_z)$ requires that $\bar{S}_{0,n}(\mathbf{k}_\perp)$ be known for all layer separations [see Eq. (7.9)]. For large layer separations, where we have no Monte Carlo information, we truncate the sum over l at $l=1$ and choose $C_0^{(n)}$ and $C_1^{(n)}$ by requiring Eqs. (9.5a) and (9.5b) to be satisfied. This leads to

$$h_{0,n}(r)=\frac{q_n}{4\nu^2}\left[1-\frac{r^2}{4}\right]\exp(-r^2/4) , \tag{9.7a}$$

$$\bar{S}_{0,n}(\mathbf{k}_\perp)=\frac{q_n|\mathbf{k}_\perp|^2}{2\nu}\exp(-|\mathbf{k}_\perp|^2) . \tag{9.7b}$$

TABLE VII. Coefficients of correlation function parametrization. $C_l^{(n)}$ is defined in Eqs. (9.1) and (9.4).

	$\|1,3,1\rangle$	$\|1,5,1\rangle$	$\|1,1,3,1,1\rangle$
$C_1^{(0)}$	1.000 000	1.000 000	1.000 000
$C_3^{(0)}$	0.350 000	1.000 000	0.450 000
$C_5^{(0)}$	−0.259 017	−0.240 000	0.548 658
$C_7^{(0)}$	−0.090 983	0.374 210	−0.498 658
$C_9^{(0)}$		−0.634 209	
$C_0^{(1)}$	1.000 000	1.000 000	1.000 000
$C_1^{(1)}$	−0.370 000	−0.400 000	−0.700 000
$C_2^{(1)}$	−1.192 373	−1.000 000	−0.227 117
$C_3^{(1)}$	0.562 373	−0.242 077	−0.072 883
$C_4^{(1)}$		0.642 077	
$C_0^{(2)}$			1.000 000
$C_1^{(2)}$			−0.300 000
$C_2^{(2)}$			−1.027 117
$C_3^{(2)}$			0.327 117

In fact, we find that Eqs. (9.7) agree remarkably well with the Monte Carlo data, except when some low relative angular momenta are excluded. $\{C_l\}$ for cases where angular momenta are not excluded are listed in Table VII. This gives a complete set of $C_l^{(n)}$, which enables us to calculate $\Delta(\mathbf{k})$ by using Eqs. (7.15) and (9.6).

In Fig. 6, we plot the correlation functions of $\bar{S}_0\tilde{}(\mathbf{k}_\perp)=\exp(|\mathbf{k}_\perp|^2/2)\bar{S}_0(\mathbf{k}_\perp)$ and $\bar{S}_1\tilde{}(\mathbf{k}_\perp)=\exp(|\mathbf{k}_\perp|^2/2)\bar{S}_1(\mathbf{k}_\perp)$ for the $|1,3,1\rangle$ state. At small $k_\perp$, one sees the parabolic form required by Eqs. (7.3) and (8.3). The coefficient of k^2 in $\bar{S}_1\tilde{}$ is negative corresponding to the negative screening charge in this layer. In Fig. 7, we plot the Fourier transform $\bar{S}\tilde{}(\mathbf{k}_\perp,k_z)$ which shows a strong peak for $k_z=\pi$ which corresponds to the screening charge alternation in the layers. This effect is characteristic of the correlated layers and would not occur in

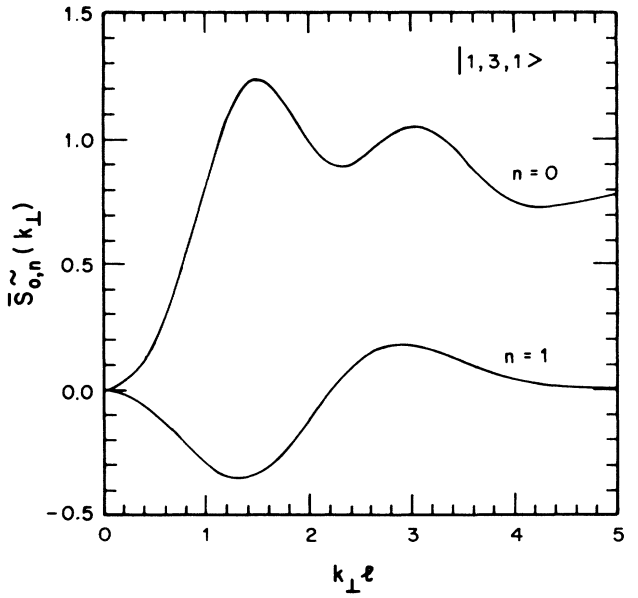

FIG. 6. $\bar{S}_0\tilde{}(\mathbf{k}_\perp)$ and $\bar{S}_1\tilde{}(\mathbf{k}_\perp)$ for the $|1,3,1\rangle$ state, as defined by Eq. (9.7a).

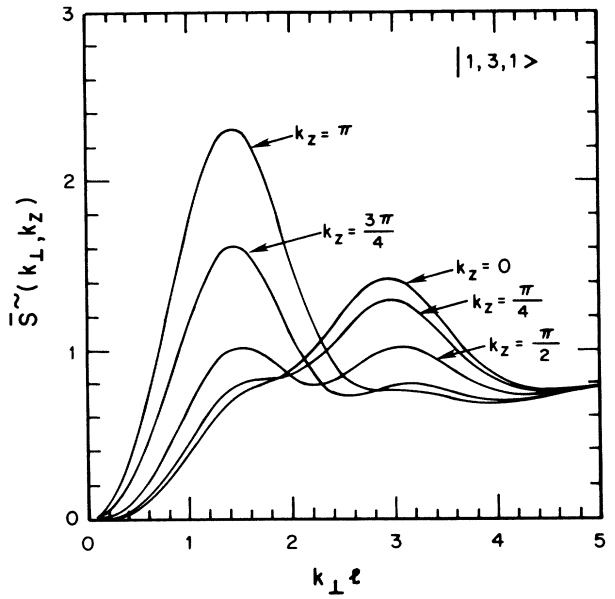

FIG. 7. The Fourier transform $\bar{S}\,\tilde{}\,(\mathbf{k}_\perp, k_z)$.

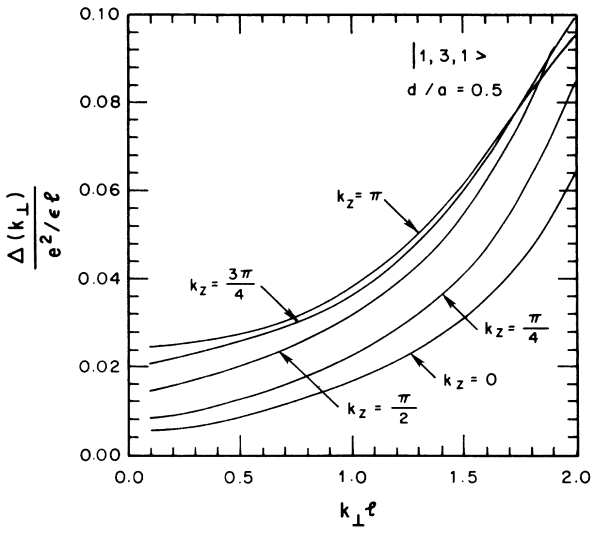

FIG. 9. Collective-excitation energies of the state $|1,3,1\rangle$ at $d/a = 0.5$, as a function of $k_\perp$ for various out-of-plane wave vectors k_z.

the $|0,5,0\rangle$ state.

The energies of the collective excitations are plotted in Fig. 8 for a separation $d/a = 0.27$ in the middle of the stability regime of the $|1,3,1\rangle$ state. Here the gap is about $0.02e^2/\epsilon l$, which is larger than the gap in the $|0,5,0\rangle$ state,[22] which is about $0.01e^2/\epsilon l$. The increases in excitation energies is consistent with the results obtained for quasihole states in Sec. V. The roton minimum characteristic of the two-dimensional state is washed out except for a few particular values of k_z. This is due to a suppression of the peak in the structure factor relative to the $|0,5,0\rangle$ state,[23] due once more to the neutralizing effect that neighboring layers have on one another. At $d/a = 0.5$, near the transition from $|1,3,1\rangle$ to $|0,5,0\rangle$, the gap becomes very small, $\sim 0.005e^2/\epsilon l$, as may be seen in Fig. 9. The roton minimum is now nowhere to be found, since at larger separations neighboring (neutralizing) layers count most heavily. The gap is now less than one-half the gap for the $|0,5,0\rangle$ state. This suggests that a discontinuous change in the gap may serve as an experimental signature for the transition between liquid states. Finally we plot $\Delta(\mathbf{k}_\perp, k_z)$ for the $|1,5,1\rangle$ state for $d/a = 0.3$ (see Fig. 10). Again, one finds a small gap $\sim 0.004e^2/\epsilon l$. The roton minimum is much more in evidence in this state, due to the stronger intralayer correlations.

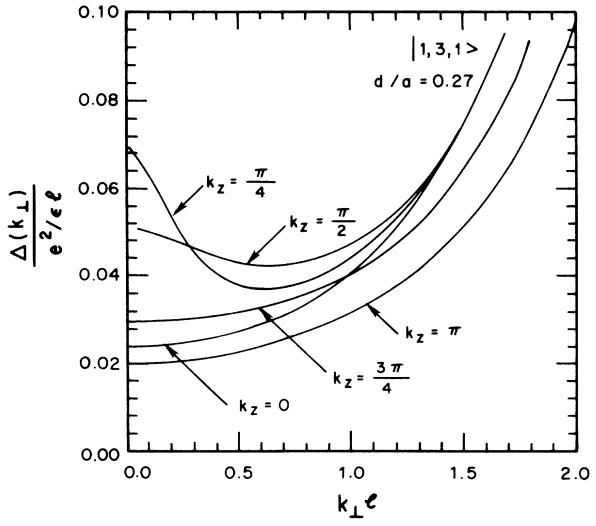

FIG. 8. Collective-excitation energies of the state $|1,3,1\rangle$ at $d/a = 0.27$, as a function of $k_\perp$ for various out-of-plane wave vectors k_z.

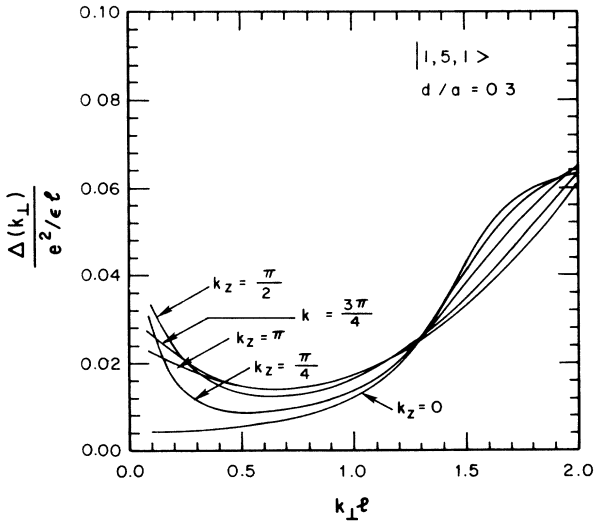

FIG. 10. Collective-excitation energies of the state $|1,5,1\rangle$ at $d/a = 0.3$, as a function of $k_\perp$ for various out-of-plane wave vectors k_z.

X. CONCLUSION

Our considerations up to this point raise a number of questions which we have deferred in order to give a unified discussion of future directions.

The first question is that of uniqueness. Are there other states, not treated in this paper, which would compete with the liquid states as ground states for the layered system? Certainly the obvious alternatives to the liquids, namely the various known types of solids, with both lateral and interlayer ordering, have been taken into account, and their domains of stability determined. However, a further possibility which we have not investigated in detail is a *combination* of staging and liquid ordering. For example, one would imagine a sequence of layers where density alternates from layer to layer. In fact, in view of the cusps in free energy which are present at special densities, it appears likely that such phases do exist. For example, a stack of identical layers with $\nu=\frac{4}{15}$ can break up into layers in the sequence $\nu_a=\frac{1}{3}$, $\nu_b=\frac{1}{5}$. Since the cusps at $\frac{1}{3}$ and $\frac{1}{5}$ are strong, there will be a competition between interlayer Coulomb and inlayer interactions. This means in general that one can expect a very different hierarchy in three dimensions than in two dimensions, even if the states with interlayer correlations are ignored. Within the class of liquid wave functions, however, it seems to be very difficult to construct other states than the ones we have considered. In the pseudopotential language, we may say that in order to exclude contributions from some V_m^α, i.e., to include a factor

$$\prod_{1\le i,j\le N}\prod_{1\le\alpha,\beta\le M}(z_{i\alpha}-z_{j\beta}),$$

it is necessary to lower the density. Any choices of these factors other than the ones we have made is inconsistent with the ordering of the V_m^α, i.e., the facts that $V_{m_1}^\alpha > V_{m_2}^\alpha$ when $m_1<m_2$ and $V_m^{\alpha_1} > V_m^{\alpha_2}$ when $\alpha_1<\alpha_2$. It therefore seems very unlikely that other liquid wave functions are possible ground states.

Finally, the experimental observability of the new phases is of course a crucial question. One general point to note is that, in two dimensions, the small total number of electrons makes measurements difficult. In fact, only transport measurements are really well developed to date. Certainly the three-dimensional nature of the transitions considered here will ease the experimental difficulties, simply because the total number of electrons is larger. In particular, measurements such as susceptibility and specific heat should be possible. The liquid-liquid transitions are of first order—they should show discontinuous changes in these properties. A striking aspect of the liquid-liquid transitions is the discontinuous change in the dielectric function at low frequencies. It should be possible to measure this by microwave techniques. In addition, we have found that the gap is discontinuous at these transitions. Measurement of this by longitudinal transport experiments suggests itself—this is in fact the only way that the spin-reversal liquid-liquid transition is detected in two dimensions.[24] It should be kept in mind that the Hall conductance itself is not expected to change at such a transition, since it is fixed by the density. Liquid-solid transitions, however could possibly be detected by this means, as well as by ultrasound.

The detection of phase transitions should be carefully distinguished from the possibility of detecting irrational charge. The latter is far more difficult, and it is hard to suggest practical experiments. The indirect method of looking at the prefactor in the hopping conductivity[25] does not work here, since it would measure the total charge on the excitation, which is rational. Rather, it seems to be necessary to look at a static charge distribution, perhaps of a pinned excitation. It is necessary to use a weak probe which does not depin the quasiparticle. Perhaps neutron scattering at very low energy, which would detect the absence of spin at the location of a quasihole, and can in principle determine the form factor, is a possibility here. Since the hole would be pinned by a charge of opposite sign, it may in fact be better to attempt to measure the spin. However, such an experiment is a long way in the future.

Thus we conclude that while the prospects for investigation of the phase diagram are good, the detection of irrational charge is likely to be difficult.

ACKNOWLEDGMENTS

This research was supported by the National Science Foundation (NSF) under Grant No. DMR-88-02383, No. DMR-88-13852, and No. PHY-82-17853, supplemented by funds from the U.S. National Aeronautics and Space Administration (NASA).

[1]D. C. Tsui, H. L. Störmer, and A. C. Gossard, Phys. Rev. Lett. **48**, 1559 (1982).

[2]R. B. Laughlin, Phys. Rev. Lett. **50**, 1395 (1983).

[3]P. K. Lam and S. M. Girvin, Phys. Rev. B **30**, 473 (1984).

[4]C. C. Grimes and G. Adams, Phys. Rev. Lett. **42**, 795 (1979).

[5]E. Y. Andrei, G. Deville, D. C. Glattli, F. I. B. Williams, E. Paris, and B. Etienne, Phys. Rev. Lett. **60**, 2765 (1988); **62**, 973 (1989); **62**, 1926 (1989); H. L. Störmer and R. L. Willett, *ibid.* **62**, 972 (1989).

[6]X. Qiu, R. Joynt, and A. H. MacDonald, Phys. Rev. B **40**, 11 943 (1989).

[7]H. L. Störmer, J. P. Eisenstein, A. C. Gossard, W. Wiegman, and K. Baldwin, Phys. Rev. Lett. **56**, 85 (1986).

[8]T. Chakraborty and P. Pietiläinen, Phys. Rev. Lett. **59**, 2784 (1987).

[9]A. H. MacDonald, Phys. Rev. B **37**, 4792 (1988).

[10]R. G. Clark *et al.*, in *Proceedings of the 18th International Conference on the Physics of Semiconductors,* edited by O. Engström (World Scientific, Singapore, 1986), p. 393; R. Willet, J. P. Eisenstein, H. L. Störmer, D. C. Tsui, A. C. Gossard, and J. H. English, Phys. Rev. Lett. **59**, 1776 (1987).

[11]B. I. Halperin, Helv. Phys. Acta **56**, 75 (1983).

[12]F. D. M. Haldane, in *The Quantum Hall Effect,* edited by S. M. Girvin and R. E. Prange (Springer, New York, 1987), Chap. 8.

[13]D. Yoshioka, A. H. MacDonald, and S. M. Girvin, Phys. Rev.

B **39**, 1932 (1989).
[14]F. D. M. Haldane, Phys. Rev. Lett. **51**, 605 (1983); F. D. M. Haldane and E. H. Rezayi, *ibid.* **54**, 237 (1985).
[15]T. Chakraborty and P. Pietiläinen, *The Fractional Quantum Hall Effect* (Springer, Berlin, 1988), Chap. 2.
[16]L. Bonsall and A. A. Maradudin, Phys. Rev. B **15**, 1959 (1977).
[17]S. M. Girvin, A. H. MacDonald, and P. M. Platzman, Phys. Rev. Lett. **54**, 581 (1985); Phys. Rev. B **33**, 2481 (1986).
[18]H. C. A. Oji, A. H. MacDonald, and S. M. Girvin, Phys. Rev. Lett. **58**, 824 (1987).
[19]See, for example, A. H. MacDonald and S. M. Girvin, Phys. Rev. B **33**, 4009 (1986).
[20]See, for example, E. M. Lifshitz and L. P. Pitaevskii, *Statistical Mechanics,* 3rd ed. (Pergamon, Oxford, 1980), Chap. 12.
[21]P. J. Forrester and B. Jancovici, J. Phys. Lett. **45**, L583 (1984).
[22]S. M. Girvin, Phys. Rev. B **30**, 558 (1984).
[23]S. M. Girvin, *The Quantum Hall Effect,* edited by S. M. Girvin and R. E. Prange (Springer, New York, 1987), Fig. 9.2.
[24]R. G. Clark *et al.*, in *Proceedings of the International Conference on Application of High Magnetic Fields in Semiconductor Physics,* edited by G. Landwehr (Springer, Berlin, 1988); J. P. Eisenstein, H. L. Störmer, L. Pfeiffer, and K. W. West, Phys. Rev. Lett. **62**, 1540 (1989).
[25]R. G. Clark, J. R. Mallett, S. R. Haynes, J. J. Harris, and C. T. Foxon, Phys. Rev. Lett. **60**, 1747 (1988).
[26]D. Levesque, J. J. Weis, and A. H. MacDonald, Phys. Rev. B **30**, 1056 (1984).